

# Carbon Nanotube Alignment via Electrohydrodynamic Patterning of Nanocomposites

Pola Goldberg-Oppenheimer, Dominik Eder, and Ullrich Steiner\*

Electrohydrodynamic (EHD) pattern formation in carbon nanotube-polymer composite films yields well-defined patterns on the micrometer scale along with the alignment of carbon nanotubes (CNTs) within these patterns. Conductive pathways in nanotube networks formed during EHD patterning of nanocomposite films results in a substantial increase in the composites' conductivity at loadings exceeding the percolation threshold. The degree of nanotube alignment can be tuned by adjusting the EHD parameters and the degree of alignment is mirrored by the conductivity across the film. Using etching techniques or by embedding relatively long nanotubes, patterned surfaces decorated by CNT brushes were generated.

## 1. Introduction

The ability to design, manufacture and control highly reliable and robust sub-micrometer patterns is of profound interest for high-performance integrated nano devices. Owing to their exceptional electric, thermal, and mechanical properties, carbon nanotubes (CNTs) have been a topic of extensive research, in particular because of their potential incorporation into easily processable and flexible polymer matrixes.<sup>[1–7]</sup> While the combination of discrete CNTs as fillers in polymers to form nanocomposites<sup>[8]</sup> results predominantly in the reinforcement of the material, the use of CNTs as scaffolds for the synthesis of inorganic replicas can be used to manufacture hybrid materials, which have a range of interesting properties.<sup>[9]</sup> In both systems, bottom-up strategies have been exploited to generate new classes of high-performance nanotube-based composite and hybrid materials, whose properties can be specifically tailored for the desired application. Nanotube-based polymer composites have potential for use in a wide range of applications, including electronic devices, solid state sensors,<sup>[7,10]</sup> electrical

interconnects, high thermal conductivity heat sinks,<sup>[11]</sup> and field-effect transistors.<sup>[12]</sup> CNT nanocomposites and hybrids have also been successfully applied in solar cells,<sup>[13–15]</sup> as photocatalysts for hydrogen production,<sup>[16]</sup> and as anode materials<sup>[17]</sup> and additives<sup>[18]</sup> in lithium-ion batteries and super-capacitors.

In order to take full advantage of the synergistic functions in CNT nanocomposites and hybrids, control of the dispersion, orientation, and interfacial chemistry of CNTs in the organic or inorganic matrix is required. Moreover, anisotropic composite structures with vertically aligned CNTs are essential to realize the full potential of nanotube-based composites both for optimization of their mechanical properties and integration into devices. For instance, while Li *et al.* demonstrated that the incorporation of CNTs in a P3HT layer<sup>[19]</sup> increased the photoconversion efficiency in a photovoltaic device caused by a faster electron transport via the nanotube network, the performance can probably be further improved by using 3D architectures with vertically aligned CNTs. In particular, nanopillar array photoelectrodes enhance the optical absorption efficiency<sup>[20,21]</sup> by enhanced collection of low-energy photons absorbed far below the surface, as compared to planar photoelectrodes.

Exfoliation routes of CNTs have been studied extensively, showing that a uniform and stable dispersion can be governed by covalent or non-covalent interactions between hydrophobic CNTs and the dispersant molecules.<sup>[22–28]</sup> Researchers have also managed to successfully align CNTs in liquid solutions upon applying an external force (e.g., electric or magnetic field, mechanical stretching, etc).<sup>[29–32]</sup> While some horizontal orientation can be achieved when CNTs are spin-cast into a thin film from a pre-aligned liquid-crystalline solution, a near complete loss of orientation is typically obtained upon their incorporation into a hosting 3D matrix.<sup>[33–35]</sup> Hence, achieving a vertically oriented nanotube network in a fully processed composite remains an important challenge. There is presently no technique to produce a well-defined CNT structure in a nanocomposite, which provides long-range control of feature positions combined with the control over CNT orientation in the composite.

In the present work we introduce a simple, versatile electrohydrodynamic (EHD) lithographic technique for patterning CNT-based polymer composites. This method provides a straightforward, single-step approach for generating high-fidelity micrometer-sized nanocomposite structures within which anisotropic CNTs are vertically aligned. The EHD concept makes use of the

P. Goldberg-Oppenheimer, Prof. U. Steiner

Cavendish Laboratory  
University of Cambridge

J. J. Thomson Avenue, Cambridge CB3 0HE, UK  
E-mail: u.steiner@phy.cam.ac.uk

D. Eder<sup>[+]</sup>

Department of Materials Science and Metallurgy  
University of Cambridge

New Museums Site, Pembroke Street, Cambridge CB2 3QZ, UK

[+] Current Address: Insitut für Physikalische Chemie, Westfälische  
Wilhelms-Universität Münster, Corrensstrasse 28/30, 48149 Münster,  
Germany

DOI: 10.1002/adfm.201002692

destabilization of thin polymer films by means of an electric field. Placing a liquified resist between parallel plates, leaving a small air gap, and applying a potential gives rise to a homogeneous electric field in the polymer layer,  $E_p$ , which causes the formation of well defined pillars with local hexagonal symmetry spanning the capacitor gap. In the presence of laterally varying  $E_p$ , i.e. when a topographically patterned top electrode is used, the EHD patterning process yields a high fidelity replication of the patterns imposed by the master top electrode. EHD lithography has previously been used to fabricate patterns in a wide variety of polymers using both featureless and topographically structured masks.<sup>[36–38]</sup> Furthermore, as EHD lithography allows to pattern most of the amorphous and semi-crystalline polymers.<sup>[38]</sup> Positional control of the generated morphologies can be adjusted by varying a number of experimental parameters, such as the initial film thickness, inter-electrode spacing,  $E_p$ -strength, surface tension and lateral periodicity of the master electrode. The degree of CNT orientation is governed by key process parameters such as the hydrodynamic flow and the strength of the applied electric field. The possibility to control self-organized patterns on the micrometer scale and the degree of anisotropy of the incorporated CNTs within the patterned nanocomposite render this technique technologically appealing.

## 2. Results and Discussion

An essential requirement for EHD patterning of CNT nanocomposites is a uniform and stable dispersion of CNTs in the host polymer matrix. Polystyrene (PS) was used as the matrix polymer for proof of concept, but nearly any polymer can be used in a similar manner. Pristine multi-walled carbon nanotubes (MWCNTs) with an average diameter of 10 nm were incorporated in PS with no additional chemical functionalization prior to the dispersion process, thereby preserving their properties. A stable and homogeneous dispersion of MWCNTs in PS was achieved using an established route described in the Experimental Section. A PS-MWCNT dispersion is shown in **Figure 1**. Microscopy observations reveal that the individual MWCNTs are decorated by PS (Figure 1B-C), sterically stabilizing the MWCNTs in solution and in the melt, aiding their efficient dispersion, while preserving their electronic and mechanical properties.<sup>[39,40]</sup> This solution was then spin-cast onto a Si-wafer substrate, which serves as an electrode in the EHD patterning process, to form a homogeneous nanocomposite film. It is important to note that at this stage no preferred orientation or alignment of MWCNTs was obtained, as confirmed by the random distribution of MWCNTs in the cross-sectional image of the composite (Figure 1D).

These composite films were then subjected to EHD patterning. The physical mechanism of the EHD pattern formation process is well-understood.<sup>[37]</sup> In short, an applied voltage across a polymer-air bilayer exerts a destabilizing electrostatic pressure  $p_{el}$  on the interface caused by interfacial polarization charges<sup>[37]</sup>

$$p_{el} = -\epsilon_0 \epsilon_p (\epsilon_p - 1) E_p^2$$

$$= -\epsilon_0 \epsilon_p (\epsilon_p - 1) \frac{U^2}{[\epsilon_p d - (\epsilon_p - 1)h]^2} \quad (1)$$

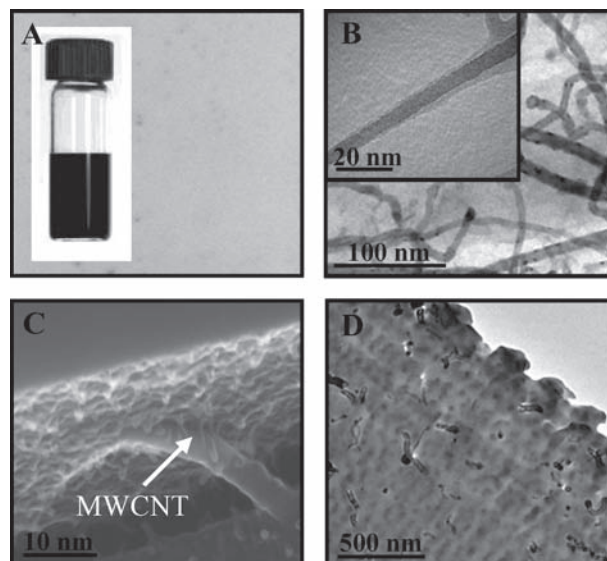


**Figure 1.** Overview of the CNT-polymer composite prior to the EHD experiment: A) Optical microscopy image of a black, stable dispersion of MWCNTs in a PS solution. B) TEM and C) SEM images of a spin-cast thin film of the MWCNT-PS composite. Inset: higher resolution TEM image, showing polymer-decorated MWCNTs. D) TEM image of a perpendicularly microtomed film of the spin-cast MWCNT-PS composite prior to EHD patterning reveals round cross-sections of MWCNTs, indicating in-plane orientation of some of the MWCNTs in the as-spun film.

where  $\epsilon_0$  is the dielectric permittivity of the vacuum,  $\epsilon_p$  is the dielectric constant of the polymer,  $h$  is local film thickness and  $d$  is the capacitor plate spacing,  $p_{el}$  prevails over the counterbalancing surface tension of air-polymer interface  $\gamma$ . Using the lubrication approximation, this gives rise to the amplification of an instability with the characteristic wavelength

$$\lambda = 2\pi \sqrt{\frac{2\gamma}{-\frac{\partial p_{el}}{\partial h}}} \quad (2)$$

The amplification of fluctuation maxima drain the surrounding polymer film, laterally detaching the individual structures, and finally forming liquid cylindrical plugs between the two electrodes. The reorganized final morphology has a local hexagonal order caused by the repulsion of the polarized wave minima and maxima. The set-up is schematically shown in **Figure 2A**, indicating the morphological reorganisation of the the MWCNT-PS composite.

Films with a typical loading of 1.5 wt% of MWCNTs were first annealed at temperatures above the glass-transition temperature of the polymer ( $T_g \approx 100$  °C), liquefying the material. Subsequently, a voltage of 120 V was applied across the electrodes, which gave rise to a laterally homogeneous electric field. This electric field causes a film instability which leads to an array of columns that span the capacitor gap. The  $1.3 \pm 0.3$   $\mu\text{m}$  high vertical pillars with an average diameter of  $1.0 \pm 0.2$   $\mu\text{m}$  are shown in Figure 2B and C. The average inter-column spacing mirrors the characteristic wavelength  $\lambda = 1.2 \pm 0.3$   $\mu\text{m}$ . The mean spacing between formed columns corresponds to the

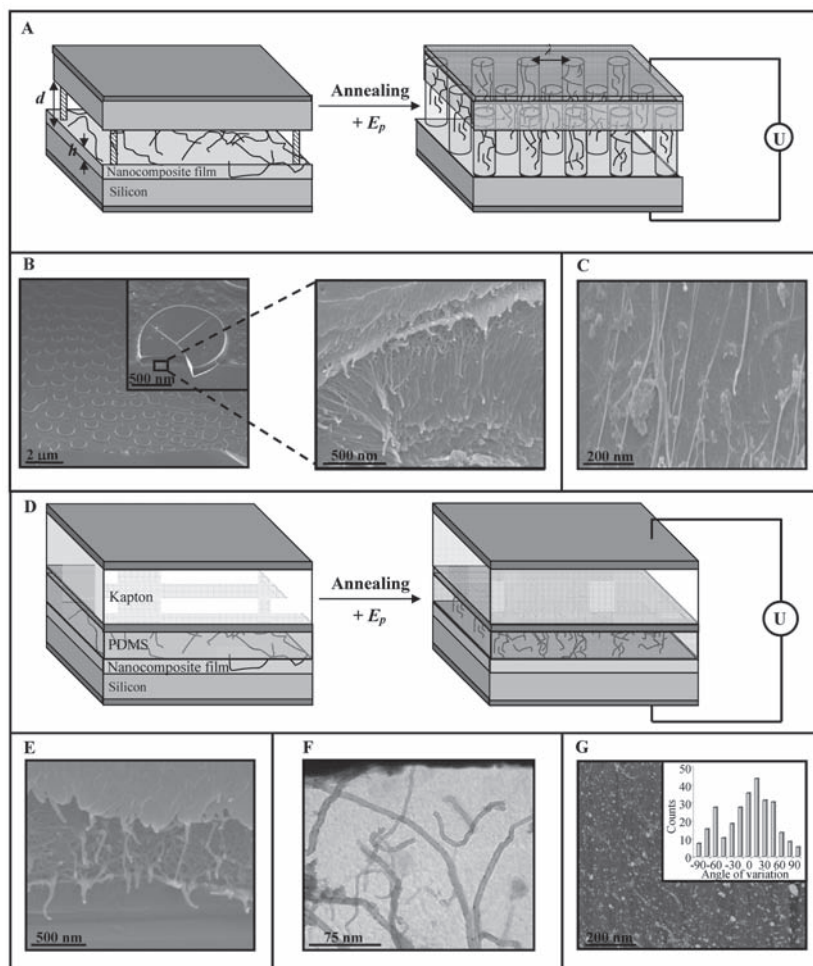


**Figure 2.** A) Schematic representation of the experimental set-up and the overall pattern formation process in a laterally homogeneous electric field. Liquefying a thin nanocomposite film with randomly dispersed MWCNTs and subsequently applying a destabilising  $E_p$  causes an EHD instability with a characteristic wavelength  $\lambda$ . Amplification of the film undulations results in pillars with local hexagonal symmetry. B) Low- and high-magnification SEM images of EHD patterned columns that contain vertically aligned MWCNTs. C) Partial removal of the PS matrix provides an improved contrast of MWCNT alignment as seen in the SEM cross section. D) Experimental configuration for exposing nanocomposite films to an electric field, in the absence of an air gap. 4 kV were applied across the Kapton, PDMS and nanocomposite film to give rise to similar electric field in the film as in (A). E–G) Cross-sections of films annealed in such a device: SEM (E), TEM (F) and AFM (G) images for an identical nanocomposite film annealed in an electric field. The histogram in (E) shows the relative MWCNT alignment with respect to electric field vector.

wavelength predicted by Equation 2. The inter-column spacing is determined by the field strength and the polymer surface tension and typically ranges from 0.5 to 30  $\mu\text{m}$  for values of  $E_p$  between  $2 \times 10^8$  and  $0.35 \times 10^8 \text{ Vm}^{-1}$  respectively, while the column diameter is a function of the initial film thickness and the plate spacing. The dimensions and lateral position of the generated patterns can be controlled by adjusting the different experimental parameters. For instance, since liquid morphologies are organized according to the ratio of the plate spacing  $d$  and the initial film thickness  $h_0$ , the variation of these two parameters determines the column height (100–1000 nm) and diameter (800 nm–3  $\mu\text{m}$ ). On the other hand, the field strength

and the polymer surface tension will dictate the position of the formed structures by establishing the characteristic wavelength, i.e. the inter-pillar spacing.

While similar patterns were obtained for different MWCNT loadings, shorter instability wavelengths and hence inter-column spacings were observed for high MWCNT loading compared to the pure polymer, reflecting a higher destabilization pressure gradient  $\partial p_{el}/\partial h$ . The origin of this effect is readily explained in terms of the dielectric properties of the composite. Similar to nanoparticles,<sup>[41]</sup> MWCNT loading increases the dielectric constant of the composite, thereby enhancing  $E_p$ .<sup>[42]</sup>

Cross-sectional examination of the pillars reveals an additional internal substructure comprised of vertically aligned MWCNTs along the axis of the columns (Figure 2B) in the direction of the electric field lines. For better imaging, the samples were subjected to plasma-enhanced etching, which selectively removed a thin polymer layer from the surface, thereby further exposing the vertical MWCNTs caused by the faster etching rate of PS. A nearly right-angle orientation of MWCNTs relative to the capacitor electrodes is seen in Figure 2C. Although short MWCNTs will align in the capacitor gap, they do not span the entire height of the formed columns. Long MWCNTs, on the other hand, align to form an interconnect between the two electrodes (see Supporting Information).

A microtomed cross section parallel to the electric field direction examined by transmission electron microscopy (TEM) and atomic force microscopy (AFM) yields additional insight into the degree of MWCNT orientation. **Figure 3** reveals that the vertically oriented MWCNTs are occasionally entangled. This is of importance with respect to the composite's electrical properties. MWCNTs, which span the entire EHD structure should have the highest conductivities for perfect vertical alignment, while shorter MWCNTs require some entanglements to ensure sufficient electrical contacts between the individual tubes that allow conduction via a percolating network. Note that the concentration of MWCNTs is higher at the surface of columns. This is most likely caused by high electric field gradients during the intermediate stage of the EHD instability: a sinusoidal undulation of a surface in a plate capacitor gives rise to a field concentration at the undulation maxima.<sup>[43]</sup> MWCNTs couple to this field gradient and experience a force in direction of the highest electric field, leading to a MWCNT accumulation in the region of the undulation that later makes contact with the upper capacitor plate, as seen in Figure 2B and Figure 3B.

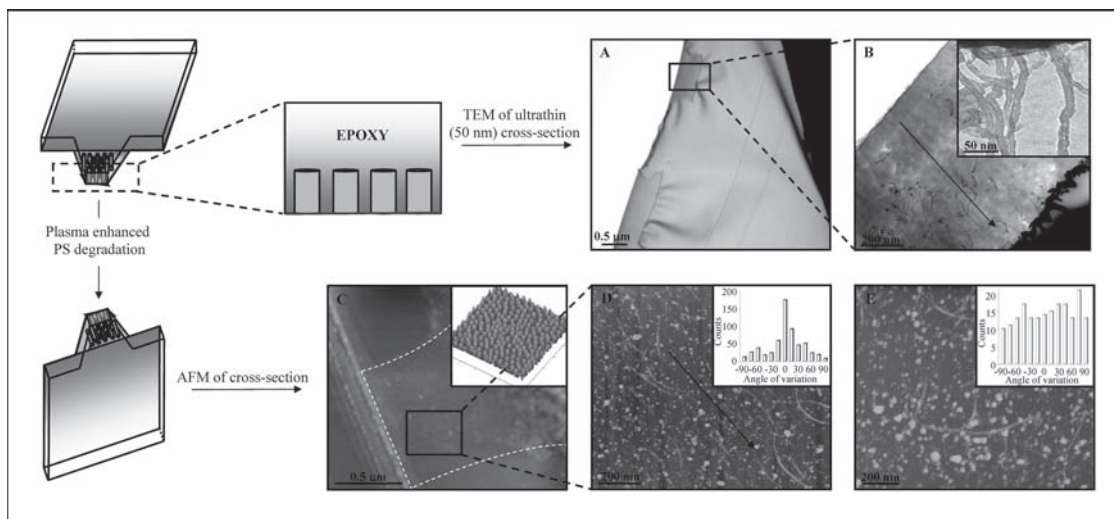


**Figure 3.** Schematic representation of sample analysis: following the embedding in an epoxy resin the lower electrode is removed, followed by microtoming ultrathin slices. A,B) and C,E) TEM and AFM ultrathin sections parallel to the direction of the electric field. Zooming into one of the columns of (A) shows the nanotube orientation in direction of the pillar axis (B, arrow), with an increased concentration of aligned MWCNTs near the top electrode (B, inset). C) AFM cross-sectional view and 3D top-view showing the columnar pattern (inset). D) High magnification AFM image of the cross-section of (C), visualizing nanotube orientation in the EHD-formed pillar. E) Cross-sectional AFM image of the as cast nanocomposite film, revealing no preferred orientation of MWCNTs. The histograms show the degree of MWCCNT alignment as an angle of variation from a cylinder axis in the patterned film (D, inset), indicated by the arrow, and from an arbitrary direction (E, inset) in the as-cast film.

To determine the average degree of MWCNT anisotropy inside EHD-formed columns, we have performed a quantitative analysis of the TEM and AFM images in (Figure 3B and D). Averaged over the entire patterned area (approx.  $200\ \mu\text{m} \times 200\ \mu\text{m}$ , averaged over 25 profiles), 80% of the MWCNTs were aligned within  $\pm 20^\circ$  of the electric field vector (Figure 3D, arrow) and 60% were within  $\pm 15^\circ$  of the director (Figure 3D, inset). This is in contrast to the as-cast nanocomposite films, where no preferred orientation was seen (Figure 3E).

The preferential MWCNT alignment along the cylinder axis can be explained by two mechanisms. Firstly, the anisotropic MWCNT structure gives rise to a dipole moment that couples to the electric field, which exerts an aligning torque on the MWCNTs. Secondly, the EHD column formation gives rise to a lateral shear flow into the columns which may act to align the MWCNTs.

To address, which of these two proposed MWCNT alignment mechanisms is dominant, a second type of experiments was performed. Instead of leaving an air gap in the capacitor, the top electrode was brought into direct contact with the nanocomposite layer (Figure 2D). In this device geometry, the electric field does not cause any flow of the composite, but results only in an aligning torque on the MWCNTs.

The results of these experiments show a somewhat lower degree of nanotube alignment (Figure 2E-G) of 45% and 37% within  $\pm 20^\circ$  and  $\pm 15^\circ$  of the electric field vector, respectively. This result indicates that the vertical orientation of the nanotubes in EHD patterned films arises from a combination of the electrostatic torque exerted on the nanotubes by the electric field and hydrodynamic convection forces and rotation by elongational component of the flow that aligns the MWCNTs during pattern formation.

The good conductivity of MWCNTs raises the question of how MWCNT alignment in the insulating PS affects the conductivity across the composite film. To investigate this, the variation of electric resistivity was measured by a four probe method at room temperature as a function of MWCNT content, for as-cast films and for EHD patterned structures, as shown in Figure 4. The introduction of 0.35 wt% of MWCNTs in an as-cast composite film lowered the resistivity by one

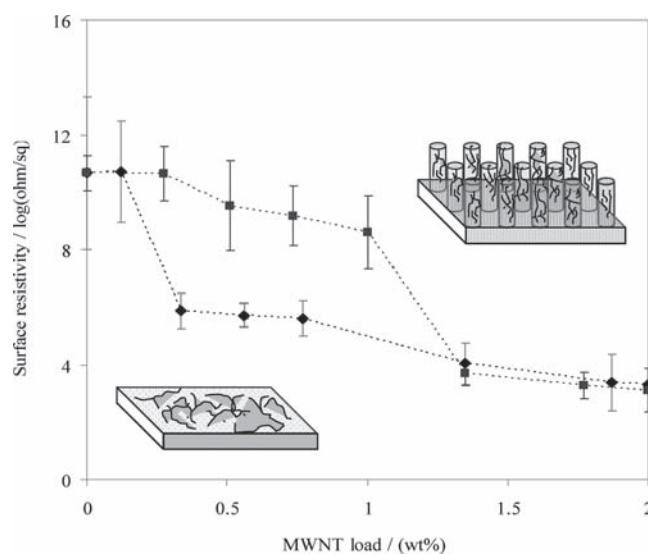


**Figure 4.** Resistivity of a spin-cast (diamonds) MWNT/PS composite film compared to an EHD-patterned nanocomposite (squares).

order of magnitude. An additional increase in MWCNT content gradually decreased the resistivity by a further factor of 10 for a MWCNT content of 2 wt%. While the conductivity of the EHD patterned sample measured along the cylinder axis (averaged over a large number of cylinders) is similar for MWCNT loadings above 1.3 wt%, the results differ for small loadings from the unpatterned film. Interestingly, the averaged (appropriately normalized) axial resistivity of EHD patterned films is higher in the 0–1.3 wt% range, in which the resistivity varies only little, with a large drop between 1 wt% and 1.3 wt%.

The difference in conductivity for MWCNT loading in the 0–1.3 wt% range can be understood in terms of a MWCNT percolation model. With a persistence length of  $\sim 300$  nm,<sup>[44]</sup> non-aligned MWCNTs are entangled. Above the percolation threshold of  $\sim 0.35$  wt% MWCNT loading, continuous conducting pathways form across the composite film. The uniaxial alignment of the MWCNTs in the EHD-generated columns reduces the number of entanglement points per chain by straightening and aligning the MWCNTs. This increases the percolation threshold to a MWCNT loading of  $\sim 1.3$  wt%. Although conductivities as high as 1 S/m have been reported for composites with a MWCNT concentration of 5.5 wt%,<sup>[45]</sup> this typically causes a short-circuit for the device used in the EHD experiments.

Finally, the embedded MWCNTs can be partially exposed upon process completion by the incomplete removal of the polymer from the top of the pillars by plasma etching. This results in a brush of vertically oriented partially free-standing nanotubes, which are supported by the remaining polymer matrix that prevents their collapse (Figure 5). Alternatively, exposed vertically standing nanotubes can also be obtained without the polymer removal step, by using MWCNTs which are longer than the height of the formed columns (Figure 5, inset). The creation of a well-defined supported CNT brush may be useful to establish an electrical circuit upon mechanically contacting plastic-based conducting composites. These hybrid vertically oriented structures therefore have potential applications for the development of flexible microelectronics, displays and biocatalytic assemblies, such as flexible

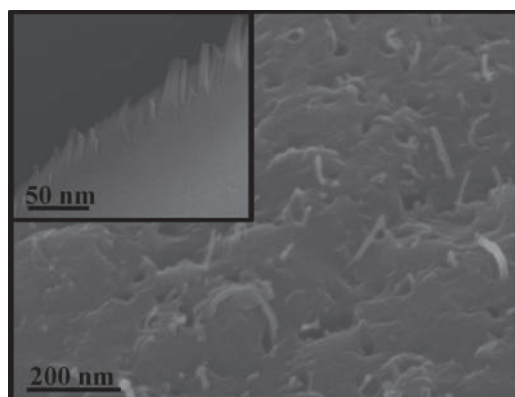


**Figure 5.** SEM top-view of partially exposed vertical MWCNTs embedded in an EHD-generated pillar. Using CNTs which are slightly longer than the pillar height results in similarly free standing nanotubes (inset).

field emitters, field emission devices (FEDs) or sensors. For example, a crucial aspect for an efficient FED is the distance between MWCNTs, which should be greater than their height to minimize the electric field screening effect. EHD generated anisotropic patterned MWCNT arrays embedded in a polymer matrix not only directly lead to the suppression of the mutual screening, but also provide a way to control both the height and distance of columns decorated with aligned MWCNTs. Oriented CNTs with exposed ends exhibit an increased electrochemically accessible surface area and high electrical conductivity. They may be used to generate well-defined electrical contacts and may provide a route for incorporating chemical functions by functionalization along their longitudinal tube axis. This is potentially useful for the development of rapid-response biochemical sensors which are selective for targeted chemical and biological molecules.

### 3. Conclusions

In summary, we have introduced a straightforward technique for the hierarchical patterning of a polymer-carbon nanotube composite by means of an electric field. EHD patterning gives rise to well-defined microscale columnar patterns with embedded MWCNTs which are uniaxially aligned parallel to the cylinder axis. With the use of a topographically patterned electrode,<sup>[37]</sup> EHD lithography allows control and manipulation of the position of the formed patterns as well as the alignment of the incorporated MWCNTs. Composite film conductivity as a function of MWCNT content shows a substantial increase in conductivity for a MWCNT loading of  $\sim 0.3$  wt%. Conductive pathways in percolating nanotube networks can be controlled by EHD patterning, shifting the percolation threshold by  $\approx 1\%$  for the field strength used in this experiment. Furthermore, the aligned MWCNTs can be exposed by selective polymer etching to form a MWCNT brush. The possibility of simultaneous structuring of the nanocomposite and control of MWCNT alignment by EHD instabilities is an intriguing way to control the properties of the composite. Despite the reduction in conductivity upon MWCNT alignment, the creation of a MWCNT-brush is of interest for establishing adhesive conducting electrical contacts, possibly paving the way for integration of nanotube-based composites into functional devices. To this end, the incorporation and alignment of CNTs into semiconducting polymer (such as P3HT) will be an interesting future direction of study.

### 4. Experimental Section

**Materials:** CVD grown MWCNTs (outer diameter: 8–15 nm, purity: higher than 95%) were purchased from Cheap Tubes Inc. Polystyrene (PS) (molecular weight: 100 and 300 kg mol<sup>-1</sup>, polydispersity < 1.07), was purchased from Polymer Standards Service GmbH, Mainz. Highly polished p-doped silicon (Si) wafers, with <100> crystal orientation (Wafernet GmbH, Eching, Germany) were used as substrates. Patterned silicon wafers were obtained from X-lith eXtreme Lithography, Ulm, Germany).

**Experimental Procedure:** The dispersion of MWCNTs in PS is facilitated by the high wettability of the aromatic PS on the graphitic MWCNT surface.<sup>[26]</sup> MWCNT-PS composites were prepared using two established procedures: a solution-evaporation method assisted by high-energy

sonication,<sup>[46,26]</sup> or block polymer stabilization of nanotubes with further incorporation inside a PS matrix.<sup>[47]</sup> Both processes yielded stable and uniform dispersions of nanotubes inside the PS matrix. For EHD experiments, a capacitor was assembled using a silicon substrate covered by a homogeneous nanocomposite film as a lower electrode. Facing it, a planar or structured Si-wafer was mounted as second electrode, leaving a thin air gap. Both capacitor electrodes were electrically contacted using silver paint (Electrodag 1415M). In some of the EHD experiments, the upper electrode was substituted by a thick Kapton CR (DuPont) sheet with a thermally evaporated 50 nm thick Au layer on the reverse side. In order to avoid the air gap and establish conformal contact with the composite film, a thin layer of poly(dimethylsiloxane) (PDMS, Sylgard 184, Dow Corning) was spin-cast and thermally crosslinked on the front side of the Kapton sheet. Since, the presence of a thick Kapton layer and a dielectric significantly lowers the effective field across the nanocomposite layer, a much higher voltage of 4 kV was applied in such an assembly. Etching in an air plasma was used to degrade PS and to partially expose the embedded MWCNTs.

**Characterization:** Scanning electron microscopy images were obtained using a LEO ULTRA 55 scanning electron microscopy (SEM) with a Schottky-emitter (ZrO/W cathode). The acceleration voltage was 15.0 kV and secondary electron images were recorded at various magnifications. Cross-sectioned surfaces for SEM investigations were prepared by fracturing the pillar array, with the fracture plane parallel to the pillar axis. A Dimension 3100 atomic force microscope (Bruker) was employed for AFM imaging to characterize patterned composite films and their cross-sections. All the measurements were performed under ambient conditions using the "Tapping Mode". "Golden Silicon Probes" cantilevers (NSG 20 with resonance frequency of 260 kHz and a force constant of 28 Nm<sup>-2</sup>) were used. For TEM cross sectional imaging, a thin layer of Pt was sputtered onto the composite films, followed by embedding into a Spurr epoxy resin. The substrate was removed and the films were sectioned using diamond knife in a Leica Ultracut Microtome, yielding sections with a thickness of 50 nm. The cross-sections were analyzed using a FEI Technai 12 transmission electron microscope (TEM) at acceleration voltage of 120 kV. The resistivity of the epoxy-embedded films was measured by a four-probe method using a Keithley 2000 voltage-current source.

## Supporting Information

Supporting Information is available from the Wiley Online Library or from the author.

## Acknowledgements

We acknowledge Kodak European Research, Cambridge for financial support. The assistance of J Rickard with the microtoming procedure is gratefully acknowledged.

Received: December 22, 2010

Revised: January 28, 2011

Published online: March 25, 2011

- [1] E. T. Thostenson, Z. Ren, T.-W. Chou, *Comp. Sci. Technol.* **2001**, 61, 1899.
- [2] X. Gong, J. Liu, S. Baskaran, R. D. Voise, J. S. Young, *Chem. Mater.* **2000**, 12, 1049.
- [3] S. Kumar, T. D. Dang, F. E. Arnold, A. R. Bhattacharyya, B. G. Min, X. Zhang, R. A. Vaia, C. Park, W. W. Adams, R. H. Hauge, R. E. Smalley, S. Ramesh, P. A. Willis, *Macromolecules* **2002**, 35, 9039.
- [4] C. Park, Z. Ounaies, K. A. Watson, R. E. Crooks, J. Smith, S. E. Lowther, J. W. Connell, E. J. Siochi, J. S. Harrison, T. L. S. Clair, *Chem. Phys. Lett.* **2002**, 364, 303.
- [5] R. H. Baughman, A. A. Zakhidov, W. A. de Heer, *Science* **2002**, 297, 787.
- [6] J. K. W. Sandler, J. E. Kirk, I. A. Kinloch, M. S. P. Shaffer, A. H. Windle, *Polymer* **2003**, 44, 5893.
- [7] R. Sen, B. Zhao, D. Perea, M. E. Itkiss, H. Hu, J. Love, E. Bekyarova, R. C. Haddon, *Nano Lett.* **2004**, 4, 459.
- [8] G. Kickelbick, *Introduction to Hybrid Materials, in Hybrid Materials: Synthesis, Characterization, and Applications*, Wiley-VCH, Weinheim, Germany, **2007**.
- [9] D. Eder, *Chem. Rev.* **2010**, 110, 1348.
- [10] S. Wong, E. Joselevich, A. Woolley, C. Cheung, C. Lieber, *Nature* **1998**, 394, 52.
- [11] S. Fan, M. G. Chapline, N. R. Franklin, T. W. Tomblor, A. M. Cassell, H. Dai, *Science* **1999**, 283, 512.
- [12] S. J. Tans, A. R. M. Verschueren, C. Dekker, *Nature* **1998**, 393, 49.
- [13] M. W. Rowell, M. A. Topinka, M. D. McGehee, H.-J. Prall, G. Dennler, N. S. Sariciftci, L. Hu, G. Gruner, *Appl. Phys. Lett.* **2006**, 88, 233506.
- [14] E. Kymakis, I. Alexandrou, G. A. J. Amaratunga, *J. Appl. Phys.* **2003**, 93, 1764.
- [15] E. Kymakis, G. A. J. Amaratunga, *Appl. Phys. Lett.* **2002**, 80, 112.
- [16] K. Dai, T. Peng, D. Ke, B. Wei, *Nanotechnology* **2009**, 20125603.
- [17] J.-i. Nakamura, Y. Sasabe, T. Takahashi, M. Inagaki, *Trans. Inst. Electr. Eng. Japan A* **1995**, 115, 349.
- [18] M. Endo, Y. Kim, T. Hayashi, K. Nishimura, T. Matusita, K. Miyashita, M. Dresselhaus, *Carbon* **2001**, 39, 1287.
- [19] C. Li, Y. Chen, Y. Wang, Z. Iqbal, M. Chhowalla, S. Mitra, *J. Mater. Chem.* **2007**, 17, 2406.
- [20] J. M. Spurgeon, H. A. Atwater, N. S. Lewis, *J. Phys. Chem. C* **2008**, 112, 6186.
- [21] L. Hu, G. Chen, *Nano Lett.* **2007**, 7, 3249.
- [22] T. Ebbesen, P. Ajayan, H. Hiura, K. Tanigaki, *Nature* **1994**, 367, 519.
- [23] Z. Jin, K. Pramoda, S. Goh, G. Xu, *Mater. Res. Bull.* **2002**, 37, 271.
- [24] B. McCarthy, J. N. Coleman, R. Czerw, A. B. Dalton, M. in het Panhuis, A. Maiti, A. Drury, P. Bernier, J. B. Nagy, B. Lahr, H. J. Byrner, D. L. Carroll, W. J. Blau, *J. Phys. Chem. B* **2002**, 106, 2210.
- [25] E. Mickelson, C. Huffman, A. Rinzler, R. Smalley, R. Hauge, J. Margrave, *Chem. Phys. Lett.* **1998**, 296, 188.
- [26] D. Qian, E. C. Dickey, R. Andrews, T. Rantell, *Appl. Phys. Lett.* **2000**, 76, 2868.
- [27] J. Sandler, M. Shaffer, T. Prasse, W. Bauhofer, K. Schulte, A. Windle, *Polymer* **1999**, 40, 5967.
- [28] H. Hiura, T. W. Ebbesen, K. Tanigaki, *Adv. Mater.* **1995**, 7, 275.
- [29] P. Ajayan, O. Stephan, C. Colliex, D. Trauth, *Science* **1994**, 265, 1212.
- [30] H. Hou, J. Ge, J. Zeng, Q. Li, D. Reneker, A. Greiner, S. Cheng, *Chem. Mater.* **2005**, 17, 967.
- [31] T. Kimura, H. Ago, M. Tobita, S. Ohshima, M. Kyotani, M. Yumura, *Adv. Mater.* **2002**, 14, 1380.
- [32] E. Thostenson, T.-W. Chou, *J. Phys. D: Appl. Phys.* **2002**, 35, L77.
- [33] B. Pradhan, R. Kohlmeyer, J. Chen, *Carbon* **2010**, 48, 217.
- [34] W. Ding, A. Eitan, F. Fisher, X. Chen, D. Dikin, R. Andrews, L. Brinson, L. Schadler, R. Ruoff, *Nano Lett.* **2003**, 3, 1593.
- [35] M. LeMieux, M. Roberts, S. Barman, Y. Jin, J. Kim, Z. Bao, *Science* **2008**, 321101.
- [36] E. Schäffer, T. Thurn-Albrecht, T. Russell, U. Steiner, *Europhys. Lett.* **2001**, 53, 518.

- [37] E. Schäffer, T. Thurn-Albrecht, T. P. Russell, U. Steiner, *Nature* **2000**, 403, 874.
- [38] P. Goldberg-Oppenheimer, U. Steiner, *Small* **2010**, 61248.
- [39] E. Nativ-Roth, R. Shvartzman-Cohen, C. Bounioux, M. Florent, D. Zhang, I. Szleifer, R. Yerushalmi-Rozen, *Macromolecules* **2007**, 40, 3676.
- [40] P. Goldberg-Oppenheimer, O. Regev, *Small* **2007**, 3, 1894.
- [41] J. Bae, E. Glogowski, S. Gupta, W. Chen, T. Emrick, T. P. Russell, *Macromolecules* **2008**, 41, 2722.
- [42] T.-E. Chang, A. Kisliuk, S. Rhodes, W. Brittain, A. Sokolov, *Polymer* **2006**, 47, 7740.
- [43] N. E. Voicu, S. Ludwigs, U. Steiner, *Adv. Mater.* **2008**, 20, 3022.
- [44] H. S. Lee, C. H. Yun, H. M. Kim, C. J. Lee, *J. Phys. Chem. C* **2007**, 111, 18882.
- [45] J. Yu, K. Lu, E. Sourty, N. Grossiord, C. E. Koning, J. Loos, *Carbon* **2007**, 45, 2897.
- [46] B. Safadi, R. Andrews, E. A. Grulke, *J. Appl. Polym. Sci.* **2002**, 84, 2660.
- [47] N. Sluzarenko, B. Heurtefeu, M. Maugey, C. Zakri, P. Poulin, S. Lecommandoux, *Carbon* **2006**, 44, 3207.
-